Available online at www.sciencedirect.com
ScienceDirect
Journal of Power Sources 164 (2007) 1–8
JOURNAL OF POWER SOURCES
www.elsevier.com/locate/jpowsour

Separation and compression characteristics of hydrogen by use of proton exchange membrane

Kazuo Onda *, Keiji Ichihara, Mitsuyuki Nagahama, Yasuo Minamoto, Takuto Araki

Department of Electrical and Electronic Engineering, Toyohashi University of Technology, 1-1 Hibarigaoka, Tempaku-cho, Toyohashi city Aich 441-8508, Japan

Received 20 September 2006; received in revised form 4 October 2006; accepted 4 October 2006
Available online 13 November 2006

Abstract

Fuel cells (FC) can produce electricity through electrochemical reaction of hydrogen with oxygen with the use of a membrane and electrode assembly (MEA). In other words, the hydrogen pressure difference between the anode and cathode can produce electricity via an electrochemical process. Conversely, when we supply electricity to MEA from an external power source, we can pump up or separate hydrogen from the low pressure anode to the high pressure cathode according to the principle of the "concentration cell". The depleted hydrogen from the FC can be recovered by the hydrogen separation pump proposed herein, or low pressure hydrogen can be pumped to high pressure hydrogen by the hydrogen compression pump proposed herein. In this study we preliminarily tested the hydrogen separation pump and hydrogen compression pump, and demonstrated their good performance. The tested performances were analyzed with the use of our simulation model of a hydrogen pump, which was made by modifying our FC simulation model, and the test results agreed well with the calculated results.

Keywords: Electrochemical hydrogen pump; Separation and compression of hydrogen; Proton exchange membrane; Concentration cell

1. Introduction

In proton exchange membrane fuel cells (PEMFCs) hydrogen and oxygen are made to flow on opposite sides of a proton exchange membrane (PEM) to induce an electrochemical reaction for getting electricity directly at the external load. Conversely, if hydrogen is made to flow at the anode supplying electricity externally, a hydrogen pump can be formed that electrochemically transports hydrogen selectively to the cathode through PEM. Hydrogen become protons at the anode of the membrane and electrode assembly (MEA), and the protons move through PEM, and at the cathode of MEA, where no air or oxygen is flowing, protons return to the higher pressure hydrogen than at the anode by combining with electrons via the external load.

We propose two applications of the hydrogen pump. The first is a hydrogen separation pump that functions mainly to selectively separate and recover hydrogen only. This can decrease the amount of hydrogen discharged from PEMFCs or other devices in places where discharge is difficult, such as deep tunnels, deep sea, or space. Moreover, the recovered hydrogen can be recycled to the intake of PEMFC and raise the fuel utilization ratio of the fuel cell. The other application is a hydrogen compression pump that functions mainly to pressurize low pressure hydrogen at the anode to high pressure hydrogen at the cathode. Hydrogen pumps are classified electrochemically as concentration cells.

To the authors' knowledge, following studies on hydrogen pumps have been reported. One is shortening the starting time of PEMFC by separation and compression of hydrogen exhausted from PEMFC by using PEM and hydrogen occlusion alloy [1]; next is also shortening the starting time of PEMFC by compressing hydrogen to 10 MPa with a PEM hydrogen compressor and storing the compressed hydrogen [2]; and the last is raising the pressure of atmospheric hydrogen to 3.5 MPa or reducing it to 0.015 MPa by using PEM [3]. However, these studies did not measure and discuss current efficiency and overpotential. Then, in the present study we experimentally investigated the basic characteristics of hydrogen pumps under various operating conditions to understand the general characteristics of hydrogen pumps. Specifically, for the hydrogen separation pump, we experimentally investigated the basic characteristics of hydro-

* Corresponding author. Tel.: +81 532 44 6722; fax: +81 532 44 6728.
E-mail address: onda@eee.tut.ac.jp (K. Onda).

0378-7753/$ – see front matter © 2006 Elsevier B.V. All rights reserved.
doi:10.1016/j.jpowsour.2006.10.018

Nomenclature

C_i	concentration of gas species i (mol cm^{-3})
D'_i	effective diffusion coefficient of gas species i (cm^2 s^{-1})
E_{Nernst}	Nernst potential (V)
F	Faraday constant (C mol^{-1})
H_i	enthalpy of gas species i (J mol^{-1})
i	current density (A cm^{-2})
i_n	current density at nth CV (A cm^{-2})
i_{ave}	average current density (A cm^{-2})
I_n	current at nth CV (A)
k	thermal conductivity (W (cm K)$^{-1}$)
k_c	condensation coefficient (s^{-1}), $k_c = 1$
M_i	molar flow rate of gas species i (mol s^{-1})
n_d	electro-osmotic coefficient of MEA
N_i	molar flux of gas species i (mol s^{-1} cm^{-2})
P_i	pressure or partial pressure of element i (Pa)
r	membrane resistance per unit area (Ω cm^{-2})
R	gas constant (J (K mol)$^{-1}$)
t_j	thickness of element j (cm)
T	operating temperature (K)
T_j	temperature at element j (K)
U	heat transfer coefficient (W cm^{-2} K^{-1})
V_{cell}	cell voltage (V)
w_j	width of element j (cm)
W_h	adiabatic compression power (W)
W_t	isothermal compression power (W)
x	distance along gas flow (cm)
y	distance perpendicular to membrane (cm)

Greek symbols

γ	specific heat ratio
η	activation overpotential (V)
η_{ohm}	resistance overpotential (V)
η_{cur}	current efficiency (%)
η_h	adiabatic compression efficiency (%)
ρ	membrane resistivity (Ω cm)

Subscripts

a	anode
c	cathode
l	liquid
v	vapor
sat	saturation
channel	flow channel

gen separation by flowing the industrial grade hydrogen at the anode and cathode, of which total pressure is atmospheric. In addition, we developed a simulation code for hydrogen pumps by improving the pseudo two-dimensional simulation code for PEMFC, and calculated the current distribution of separation pump cells, and compared this with the measured current distribution at a segmented electrode cell. For the compression pump, we experimentally clarified the hydrogen pressurization characteristics up to a cathode pressure of 1 MPa. At that time, we also investigated the problem of hydrogen cross leak by changing the pumping rate of hydrogen (current density of pump cell) and cathode pressure.

2. Operating principle of hydrogen pump

Fig. 1 shows the operating principle of the hydrogen pump. When the electricity is supplied to the moderately moistened MEA, the hydrogen is pressurized from the low pressure anode to the high pressure cathode. At the anode and cathode of the MEA, the electrochemical reactions shown in Eqs. (1) and (2) proceed at the contact interface of catalyst electrode and PEM, and Eq. (3) holds for the total reaction [4].

$$\text{Anode}: \ \mathrm{H_2}(P_a) \rightarrow 2\mathrm{H^+} + 2\mathrm{e^-} \tag{1}$$

$$\text{Cathode}: \ 2\mathrm{H^+} + 2\mathrm{e^-} \rightarrow \mathrm{H_2}(P_c) \tag{2}$$

$$\text{Total reaction}: \ \mathrm{H_2}(P_a) \rightarrow \mathrm{H_2}(P_c) \tag{3}$$

Cell voltage V_{cell} in which hydrogen is pressurized from partial pressure P_a to partial pressure P_c is described by Eq. (4) following a concentration cell with temperature T.

$$V_{\text{cell}} = E_{\text{Nernst}} + ir + \eta, \quad E_{\text{Nernst}} = \frac{RT}{2F} \ln \frac{P_c}{P_a} \tag{4}$$

The first term of the right-hand side of Eq. (4) is called the Nernst potential E_{Nernst}, and since in a real cell there is activation overpotential and membrane resistance, V_{cell} is larger than the ideal E_{Nernst}. In the hydrogen separation pump, the total pressure at anode is equal to that at cathode, but the hydrogen partial pressure P_a at anode is smaller than the partial pressure P_c at cathode. In the hydrogen compression pump, the total pressure at cathode is larger than that at anode, with $P_a < P_c$ [5].

At the cathode of PEMFC, since H^+ reacts with oxygen to produce water via a 4-electron electrochemical reaction, the activation overpotential η is large such as about 0.3 V, but there are almost no reports on the η at cathode of hydrogen pump where H^+ returns to H_2. Since the anode of hydrogen pump is the same as PEMFC, η seems to be small similarly to PEMFC. In addition,

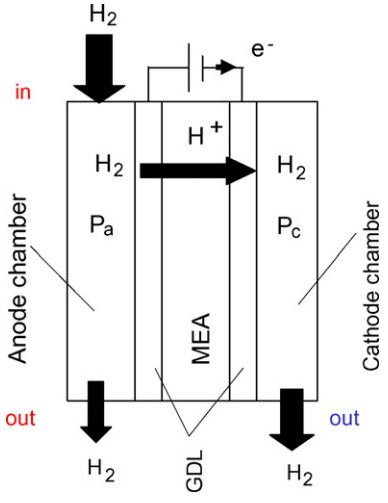

Fig. 1. Operating principle of H_2 pump.

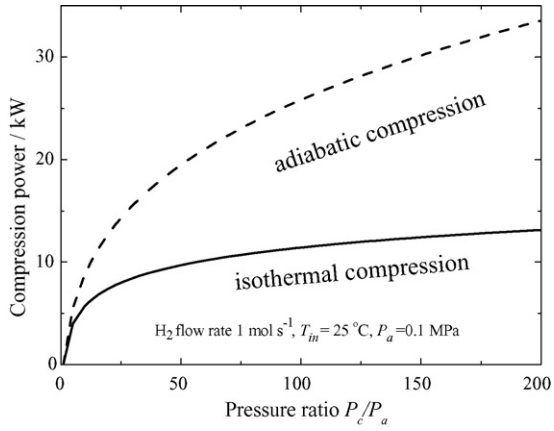

Fig. 2. Comparison of powers for isothermal and adiabatic compression of 1 mol s^{-1} H_2.

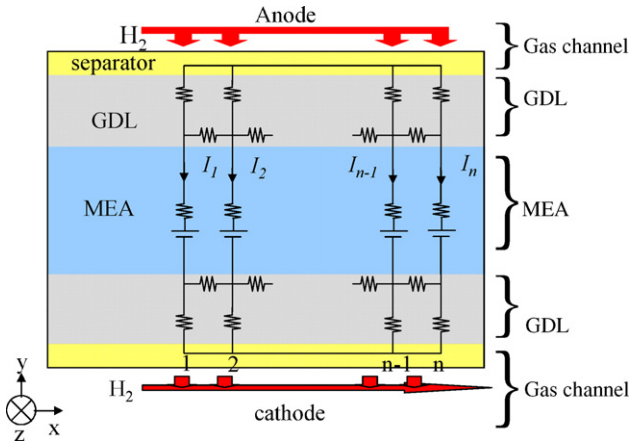

Fig. 3. Equivalent circuit of H_2 pump.

since in a PEMFC hydrogen is expanded isothermally following the action of a concentration cell, in a hydrogen pump it is similarly compressed isothermally as described with E_{Nernst} of Eq. (4). Thus, whereas the power of hydrogen mechanical compressor is described by the adiabatic process of Eq. (5), the power of hydrogen pump is described by the isothermal process of Eq. (6). Note that Eqs. (5) and (6) show the power for hydrogen flow rate of 1 mol s^{-1}.

Adiabatic compression power:

$$W_h = \frac{\gamma}{\gamma - 1} RT \left[\frac{P_c^{(\gamma-1)/\gamma}}{P_a} - 1 \right] \tag{5}$$

Isothermal compression power:

$$W_t = RT \ln \frac{P_c}{P_a} \tag{6}$$

Fig. 2 compares the compressor powers of Eqs. (5) and (6) versus the compression ratio P_c/P_a. In comparing the ideal powers with no loss, the isothermal compression power is about half of the adiabatic compression power. It means that this hydrogen pump can become an energy saving compressor. In Fig. 2, the ratio of specific heat γ is 1.4, P_c/P_a is the compression ratio, and T_{in} is room temperature of 25 °C. A gas turbine cycle where the compression and expansion processes are isothermal is called the Ericsson cycle, and in the alkali metal thermoelectric energy conversion (AMTEC) [6] Na metal flows in this isothermal compression/expansion process.

3. Analysis of hydrogen pump

3.1. Analytical model

The power generation characteristics of PEMFC have been analyzed with many calculation programs. The hydrogen pump does not have so complex processes as PEMFC, so the PEMFC simulation code [7] was simplified to provide a simulation code for hydrogen pump. To confirm the reliability of this simulation, the current distribution was measured in a segmented electrode cell similarly to PEMFC [7], and was compared with the calculated current distribution. The analysis is pseudo two-dimensional along the gas flow direction (x) of channel and perpendicular to the MEA (y), and the mass/charge and energy conservation equations were simultaneously solved with an equivalent circuit of hydrogen pump shown in Fig. 3. The basic equations were discretized with the control volume (CV) method [8]. The number of CV along x direction was optional, and the CV number along y direction was 5, i.e., the respective channels and GDLs of the anode and cathode, and the MEA. The separator was assumed to be equipotential. Non-isotropic resistance of the gas diffusion layer (GDL) along the x and y direction was used according to the measured values. Various quantities along the z direction perpendicular to the xy plane were assumed to be uniform, and in a serpentine flow on x–z plane the z direction length was substituted for the x direction. The flow in the channel was assumed to be a plug flow, and since the constant temperature water was supplied through the separator, the separator temperature was assumed to be constant. The membrane properties such as diffusion coefficient and electro-osmotic coefficient of water through MEA were measured [9] for our membrane to be adopted in the following calculation.

3.2. Mass/charge balance

Fluid in the channel and GDL was assumed to flow in a gas–liquid two-phase state, and the supplied and transported hydrogen and water was assumed to flow in the x direction in the channel and in the y direction in the GDL. The portion of water vapor that exceeded the saturated vapor pressure was assumed to condense and move with the same velocity as the fluid. Hydrogen diffusion along the x direction is also considered. The flow divided in each CV was assumed to be a plug flow with constant velocity, concentration of chemical each species, and temperature. The cross-leak of hydrogen was not considered in our analysis. The mass and charge conservation equations are as follows. The condensation coefficient k_c is assumed to be 1.

Anode:

$$\frac{dM_{H_2}}{dx} = -w_{\text{channel}} \cdot N_{H_2} = -\frac{w_{\text{channel}} \cdot i_n}{2F} - D'_{H_2} \frac{d^2 C_{H_2}}{dx^2} \tag{7}$$

$$\frac{dM^{l}_{H_2O,a}}{dx} = \left(\frac{k_c \cdot w_{channel} \cdot t_{channel}}{RT_a}\right) \times \left(\frac{M^{v}_{H_2O,a}}{M^{v}_{H_2O,a} + M_{H_2} + M_{N_2}} P - P^{sat}_{H_2O,a}\right) \quad (8)$$

$$\frac{dM^{v}_{H_2O,a}}{dx} = -\frac{dM^{l}_{H_2O,a}}{dx} - w_{channel} \cdot \left(\frac{i_n}{F} \cdot n_d - D'_{H_2O} \frac{dC_{H_2O}}{dy}\right) \quad (9)$$

Cathode:

$$\frac{dM_{H_2}}{dx} = w_{channel} \cdot N_{H_2} = \frac{w_{channel} \cdot i_n}{2F} \quad (10)$$

$$\frac{dM^{l}_{H_2O,c}}{dx} = \left(\frac{k_c \cdot w_{channel} \cdot t_{channel}}{RT_c}\right) \times \left(\frac{M^{v}_{H_2O,c}}{M^{v}_{H_2O,c} + M_{H_2} + M_{N_2}} P - P^{sat}_{H_2O,c}\right) \quad (11)$$

$$\frac{dM^{v}_{H_2O,c}}{dx} = -\frac{dM^{l}_{H_2O,c}}{dx} + w_{channel} \cdot \left(\frac{i_n}{F} \cdot n_d - D'_{H_2O} \frac{dC_{H_2O}}{dy}\right) \quad (12)$$

3.3. Energy balance

Heat conduction and heat transfer in the x and y directions, enthalpy flux, heat generation by overpotentials, and latent heat of evaporation were considered in each region of the anode channel, anode GDL, MEA, cathode GDL, and cathode channel. The quasi-two-dimensional energy conservation equations are shown as follows. Most of the heat generated at MEA was conducted through GDL to the separator of which temperature was kept constant by the circulating water of constant temperature, so in most cases both the MEA and GDL had almost equal temperature to the separator within 2 °C.

Flow channel:

$$t_{channel} \cdot w_{channel} \frac{d}{dx}\left(\kappa_{gas,k} \frac{dT}{dx}\right) = -\frac{d}{dx}\sum_i M_i \cdot H_{i-gas,k} + w_{channel}\sum_i N_i \cdot H_{i-gas,k} - w_{channel} \cdot U_{gas,k-GDL,k}(T_{GDL,k} - T_{gas,k}) - (w_{channel} + 2t_{channel}) \cdot U_{gas,k-separator}(T_{channel} - T_{gas,k}) \quad (13)$$

GDL:

$$t_{GDL} \cdot w_{separator} \frac{d}{dx}\left(\kappa_{GDL,k} \frac{dT}{dx}\right) = w_{channel}\sum_i N_i (H_{i-gas,k} - H_{i-GDL,k}) - \sum_i w_i \cdot k_{GDL,k-i}\left(\frac{T_{GDL} - T_i}{dy}\right) - w_{channel} \cdot t_{GDL} \cdot \rho_{GDL} \cdot i_n^2 - w_{channel} \cdot U_{gas,k}(T_{gas,k} - T_{GDL,k}) \quad (14)$$

MEA:

$$t_{MEA} \cdot w_{separator} \frac{d}{dx}\left(\kappa_{MEA} \frac{dT}{dx}\right) = w_{channel}\sum_i N_i \cdot H_{i-GDL,k} - \sum_k w_{channel} \cdot k_{GDL,k-MEA}\left(\frac{T_{MEA} - T_{GDL,k}}{dy}\right) - w_{channel} \cdot i_n(\eta + \eta_{ohm}) \quad (15)$$

4. Experimental apparatus and constitution of single cell

Fig. 4 shows the schematic diagram of our experimental apparatus. H_2 (in some instances mixed with N_2) was supplied to the anode inlet, but the cathode inlet was closed so that nothing was supplied. After the flow rate of H_2 was adjusted, H_2 was humidified in a humidifier and supplied to the anode of hydrogen pump cell. Voltage was applied to the cell, and the voltage–current density (V–i) characteristics were measured. The flow rate of H_2 transported to the cathode was measured by a soap film flow meter, after the moisture of cathode gas was eliminated in a gas–liquid separator. The MEA resistance was measured with an LCR meter of which frequency was set to 1 kHz, including its contact resistance. Industrial grade of H_2 with a purity of over 99.99% was supplied.

The structure of the hydrogen pump cell is nearly the same as a fuel cell [7], and the gas channel is of a single serpentine type. The cell was tested with the MEA standing vertically, and gas flowed vertically from the top to the bottom so that condensed water might not accumulate. The effective electrode area of the cell was 10 cm^2, and carbon paper with thickness of 200 μm was placed on either side of MEA as a GDL, and the periphery of GDL was sealed with a silicone sheet so that H_2 did not leak. The MEA and GDL were sandwiched between two separators grooved by channels, and constant temperature water was supplied to the separator to keep the cell temperature constant [7].

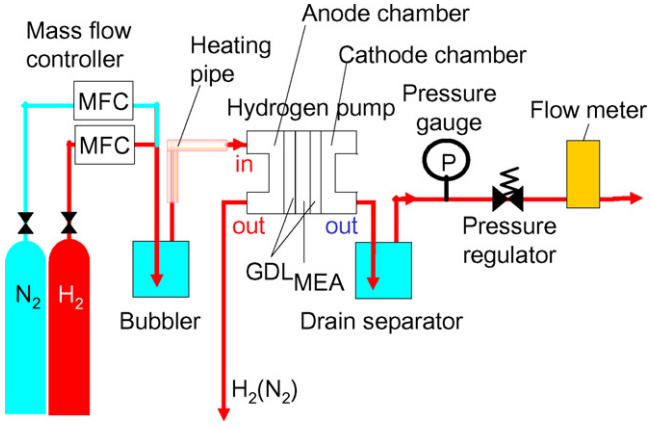

Fig. 4. Schematic diagram of experimental apparatus.

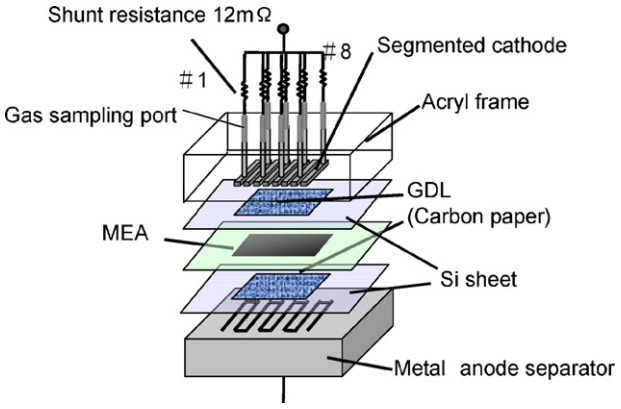

Fig. 5. Schematic diagram of segmented electrode cell.

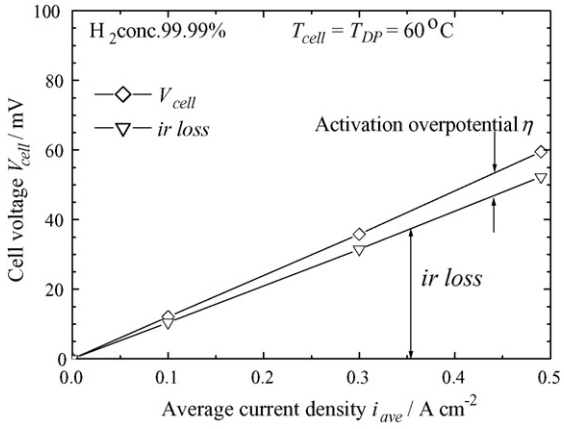

Fig. 6. Basic V_{cell}–i_{ave} characteristics of atmospheric H_2 pump cell.

In a hydrogen separation test in which the hydrogen concentration was changed, the cell clamp pressure was taken to be 1 MPa, and N_2 was mixed with a constant flow rate of H_2 to change the hydrogen concentration at anode. The hydrogen separation test was conducted under atmospheric pressure for both the anode and cathode. In a hydrogen pressurization test, the cell clamp pressure was raised to 3 MPa to prevent gas leaks from the cell. By setting a backpressure valve at cathode outlet, the cathode pressure was regulated from atmospheric pressure to 1 MPa, which is not subjected to the high pressure gas production regulations. The anode at this time was set at atmospheric pressure. Since the large pressure was exerted on the MEA and GDL, care was taken to avoid the damage of MEA and GDL by the large pressing force into the flow channel or gas supply hole. To experimentally confirm the calculated results for the hydrogen pump, the current distribution of the cell was measured with the segmented electrode cell shown in Fig. 5. The shunt resistor of 12 mΩ, which was 1 digit smaller than the membrane resistance (about 100 mΩ), was connected to each of the segmented eight electrodes to measure the current distribution from the voltage drops through the shunt resistors.

5. Test of hydrogen pump and comparison with analysis

5.1. Basic test of hydrogen pump

First, keeping the anode and cathode of the hydrogen pump at atmospheric pressure, 38.0 cc min^{-1} (at 25 °C and 101.3 kPa) of industrial grade hydrogen was supplied at the same humidification temperature as the cell temperature. The V_{cell}–i_{ave} curve and *ir* loss of the cell were measured as the basic characteristics of hydrogen pump as shown in Fig. 6. Here the supplied H_2 flow rate of 38.0 cc min^{-1} was corresponding to the hydrogen transport rate of 100% at $i_{ave} = 0.5$ A cm^{-2}, which was defined as the ratio of the H_2 flow rate determined by the supplied current to the supplied H_2 flow rate. In Fig. 6 both the cell temperature and anode humidification temperature were 60 °C. In this figure the relation between i_{ave} and V_{cell} are linear, and V_{cell} is small, about 60 mV, at $i_{ave} = 0.49$ A cm^{-2}. Under this experimental condition the Nernst potential was calculated to be small, about 0.2 mV, from the H_2 partial pressures at anode and cathode taking into account their water vapor pressures. Therefore, the activation overpotential η was seen to be the value obtained by subtracting *ir* loss from V_{cell} in Eq. (4).

Next, under these conditions the H_2 flow rate measured at the cathode outlet is shown in Fig. 7 as the flow rate of H_2 transferred from the anode to the cathode. The relation between the transferred flow rate and i_{ave} are linear, and moreover the measured flow rate matches the H_2 flow rate by Faraday's law. Thus, it is seen that the H_2 equivalent to the supplied current is transferred to cathode. The ratio of the measured flow rate to the H_2 flow rate given by the supplied current in use of Faraday's law is shown in Fig. 7 as the current efficiency η_{cur}. At each current density η_{cur} is nearly 100%.

5.2. Hydrogen compression test

Following the basic test of hydrogen pump in the preceding section, a test was conducted in which H_2 was compressed electrochemically up to higher pressure $P_{cathode}$ at cathode than the anode pressure P_{anode}, similarly to a mechanical compressor. This differed from the basic test in that $P_{cathode}$ was raised up to 1 MPa, which was higher than the P_{anode} of atmospheric pressure, but other conditions were the same. The *V*–*i* characteristics obtained in this hydrogen compression test are shown

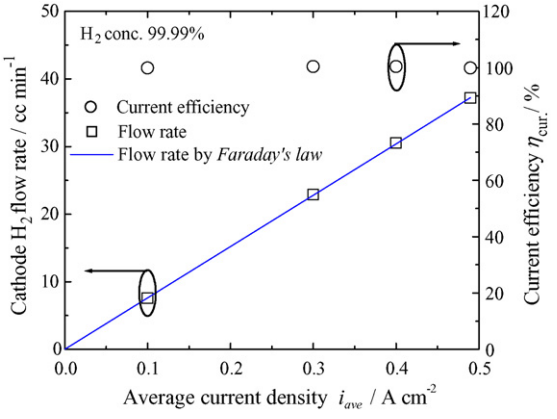

Fig. 7. Flow rate of H_2 transferred to cathode and current efficiency of atmospheric H_2 pump cell.

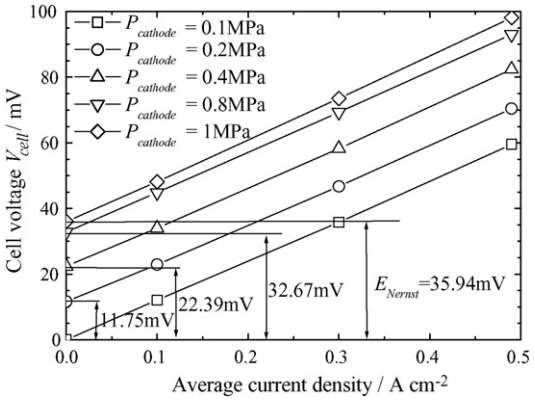

Fig. 8. Change of V_{cell}–i_{ave} characteristics by cathode pressure of H_2 compression pump.

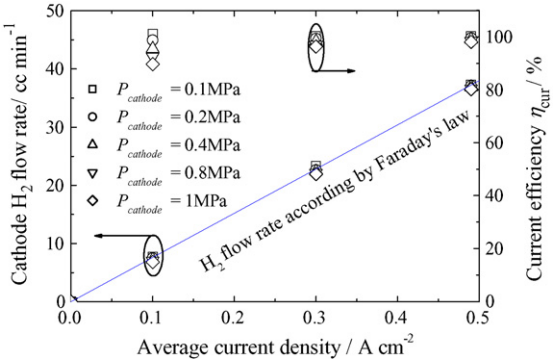

Fig. 10. Flow rate of H_2 transferred to cathode and current efficiency of H_2 compression pump.

in Fig. 8. Similarly to Fig. 6, i_{ave} and V_{cell} are in a linear relationship, and when $P_{cathode}$ is raised the open circuit voltage also increases. Since this increase in open circuit voltage agrees well with E_{Nernst} from Eq. (4) as shown in Fig. 8, it is seen that this increase is due to E_{Nernst}. When $P_{cathode}$ is 1 MPa, E_{Nernst} becomes 36 mV. The *ir* loss measured at this time and η obtained from Eq. (4) are shown in Fig. 9 as functions of i_{ave}. There is almost no dependence of these losses on $P_{cathode}$, and it is seen that η is small and *ir* loss is dominant. This η also agrees well with the η in the basic test.

The flow rate of H_2 transferred to cathode in the experiment shown in Fig. 8 is shown in Fig. 10 with the η_{cur} calculated from the flow rate. The flow rate of H_2 transferred to cathode almost obeys Faraday's law, but η_{cur} tends to decrease when $P_{cathode}$ increases. When i_{ave} is low, η_{cur} also trends to decrease. Considering that the H_2 transferred rate increases with i_{ave}, and that the cross-leak rate through MEA is supposed to be proportional to the pressure difference $P_{cathode}$–P_{anode}, the real H_2 transfer rate increases with i_{ave}. Since the cross-leak rate was still being measured in change of operating conditions, we would like to report the cross leak at another time.

As mentioned above, the major losses of the hydrogen compression pump could be measured, so the theoretical compression powers compared in Fig. 2 were discussed considering adiabatic efficiencies as shown in Fig. 11. Fig. 11 shows a comparison between the adiabatic compression powers with adiabatic efficiencies η_h of 0.7 and 1, the ideal isothermal compression power, and the real power of hydrogen compression pump including the *ir* and η losses measured at i_{ave} = 0.1 A cm^{-2}, where the abscissa is compression ratio P_c/P_a. Since the loss proportion becomes small when P_c is high and i_{ave} is small (see Eq. (4)), the compression power with high P_c and low i_{ave} approaches the ideal isothermal compression power. The hydrogen pump in this report has about 1.6 times the ideal isothermal compression power when P_c/P_a = 10 and i_{ave} = 0.1 A cm^{-2}, which is nearly equal to the ideal adiabatic compression power. Thus, while development issues remain, this hydrogen pump is able to become an energy saving compressor.

5.3. Hydrogen separation test

When attempting to recover H_2 from the depleted anode gas of PEMFC, its H_2 concentration will probably change considerably. We therefore conducted the hydrogen separation test by changing the H_2 concentration. Here the anode and cathode total pressure was atmospheric, and the H_2 flow rate at anode was con-

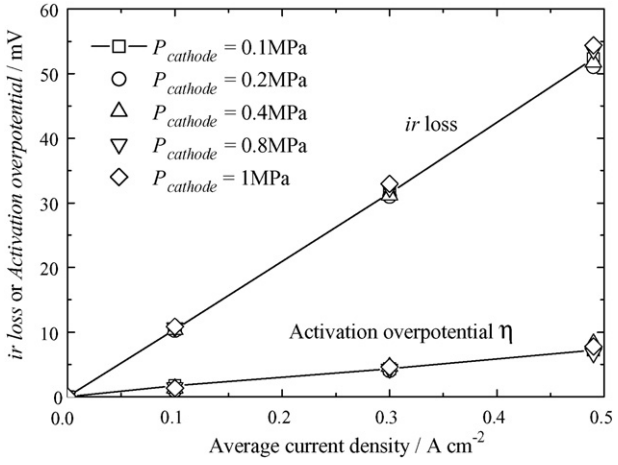

Fig. 9. Change of *ir* and η losses vs. i_{ave} by cathode pressure of H_2 compression pump.

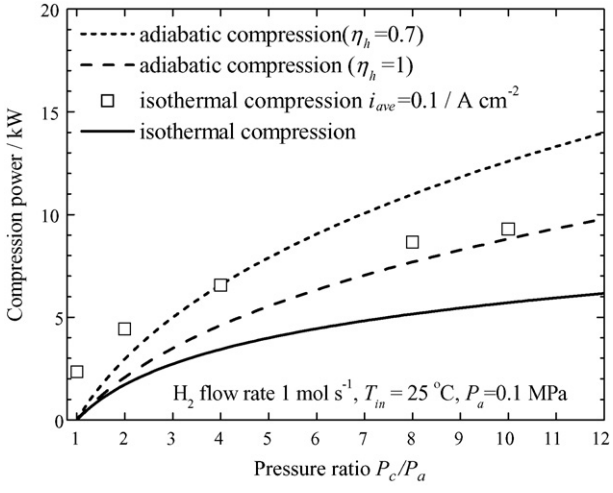

Fig. 11. Comparison of compression powers for isothermal and adiabatic compression of 1 mol s^{-1} H_2.

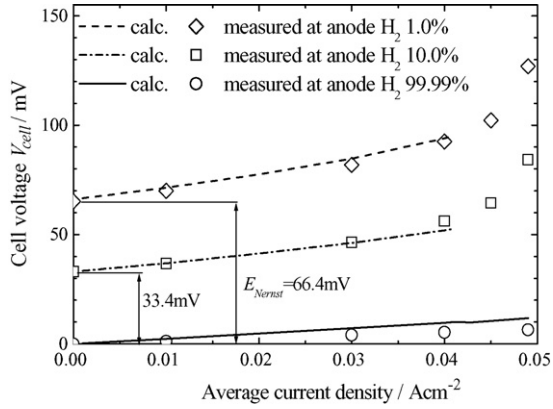

Fig. 12. Change of V_{cell}–i_{ave} characteristics by H_2 concentration of H_2 separation pump.

stant at 3.8 cc min^{-1}, 1/10 of that in the preceding section, and was diluted by N_2. i_{ave} was also 1/10, so at 0.05 A cm^{-2} the hydrogen transport rate was 100%. Other test conditions were the same as in the preceding section. The V_{cell}–i_{ave} characteristics are shown in Fig. 12 when the anode H_2 concentration was changed to 99.99, 10, and 1%. When H_2 concentration is high and i_{ave} is low, the relation between i_{ave} and V_{cell} is linear, but when H_2 concentration becomes lower and i_{ave} becomes higher, V_{cell} becomes larger than the linear line. Including the open circuit voltage the overall V_{cell} increases with decrease of H_2 concentration. This increase is due to the Nernst potential E_{Nernst}. The open circuit potential E_{Nernst} is calculated to be 33.4 mV for a 10% H_2 concentration, and 66.4 mV for a 1% H_2 concentration, in good agreement with the measured values. The reason for why V_{cell} rises rapidly as i_{ave} becomes larger is thought to be that E_{Nernst} increases at downstream of anode due to the decreasing H_2 concentration. The *ir* loss measured at the concentration change test of Fig. 12 showed very little change, and was proportional to i_{ave}.

The measured flow rate of H_2 transferred to cathode is shown in Fig. 13 together with the current efficiency η_{cur}. Regardless of the H_2 concentration, H_2 is transported to cathode according Faraday's law, and η_{cur} obtained from the transferred flow rate is about 100%. In this way, 98% of H_2 was recovered at about 130 mV from the anode exhaust gas of 1% H_2 concentration. If the recovered H_2 of high concentration can generate electricity at 700 mV in PEMFC, it is very beneficial to separate and recover the dilute anode H_2 exhausted from PEMFC by use of the hydrogen separation pump. However, when high concentration CO remains in the exhaust gas, there is a problem of catalyst poisoning.

5.4. Calculation of current distribution at hydrogen separation pump cell and its comparison with measurements

As mentioned in the preceding section, the hydrogen separation pump shows complex behavior since the H_2 concentration declines at the downstream of anode with increasing E_{Nernst}. Current distribution was then calculated using η of Fig. 9 with the method described in Section 4, and compared with the current distribution measured by the segmented electrode cell of Fig. 5. Fig. 14 shows a comparison of the calculated and measured results under the parameter of i_{ave} when H_2 concentration is 1%. The measured value is slightly larger than the calculated at inlet region where i_{ave} is large, but the analytical results agree well with the measurements. In the basic test of hydrogen pump described in Section 5.1, the current distribution was also measured and analyzed. Since E_{Nernst}, membrane resistance, and η became constant along the flow, both the measured and analytical current distributions were constant with i_{ave} along the flow, they are not shown and discussed here.

The potential distribution of the cell inside along the gas flow direction (x) was calculated for a case of i_{ave} = 0.04 A cm^{-2} in Fig. 14, and the distribution is shown in Fig. 15 together with current distribution. Because the anode H_2 concentration is decreasing toward the cell outlet, E_{Nernst} is increasing and almost all of V_{cell} is represented by E_{Nernst}, resulting that E_{Nernst} is nearly equal to V_{cell} at the vicinity of outlet. The next governing factor is *ir* loss, and the effect by activation overpotential η is small. Here it should be noted that the membrane resistance of MEA is nearly constant, as will be described below, but since the short-circuit current in the x direction of GDL cannot be ignored, the current which flows through the shunt resistance of 12 mΩ in Fig. 15 (broken line and this current was compared

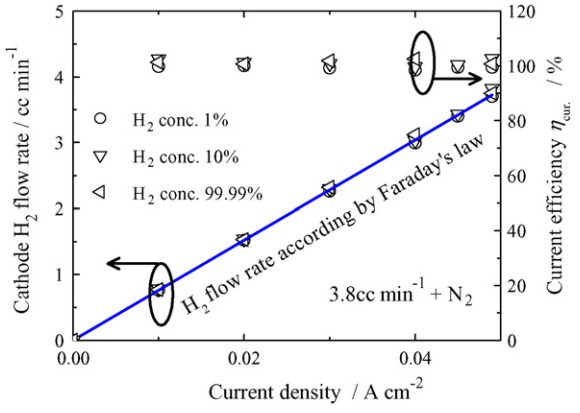

Fig. 13. Flow rate of H_2 transferred to cathode and current efficiency of atmospheric H_2 separation pump.

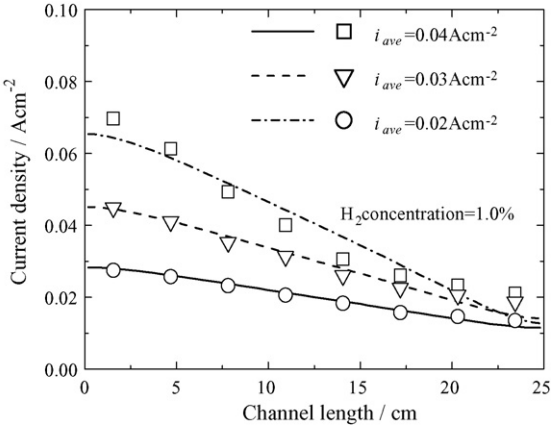

Fig. 14. Comparison between calculated and measured current distributions of H_2 separation pump.

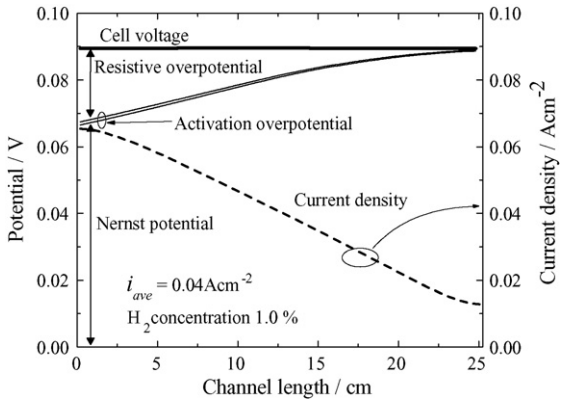

Fig. 15. Calculated potential distributions along channel flow of H_2 separation pump (i_{ave} = 0.04 A cm^{-2}, H_2 concentration = 1%).

with the measurement) becomes slightly larger than the current through MEA (this current gives *ir* loss) at the cell downstream. Fig. 12 compares the calculated lines of V_{cell} by this analysis with the measured V_{cell}. The H_2 diffusion and short circuit by GDL along the flow direction (x) become serious in the vicinity of cell outlet when the H_2 concentration is low, and currently there is not a good agreement between the calculated and measured results in Fig. 12. Further investigation will be needed in the future.

Water vapor in the anode hydrogen is transferred to the cathode side by electro-osmosis, and it returns to the anode side by the back diffusion determined by the pressure difference of water vapor between the two electrodes. To investigate the water behavior in hydrogen pump, the wetness fraction of cathode flow and the relative humidity of anode flow along the x direction were calculated and discussed under the experimental conditions of Fig. 15. Here, the wetness fraction is defined as (total molar flow rate of vapor and condensed water)/(molar flow rate of vapor) of the flow in channel. Since the water vapor transport from anode to cathode by electro-osmosis exceeded the back diffusion of water vapor from cathode to anode, the cathode wetness fraction was about 7 at inlet and decreasing to about 5 at the outlet, while the relative humidity at anode decreased from 100% at inlet, which was determined by the humidification conditions of supplied gas, to 97% at outlet. The membrane resistance of MEA showed almost no change under this calculated water behavior, and the *ir* loss shown in Fig. 15 was determined by the current distribution.

With regard to the temperature distribution calculated from the energy balance equation, in many cases the heat generated by overpotentials at MEA was mainly conducted through GDL to the separator which temperature was kept constant by circulating constant temperature water, so the temperatures of MEA and GDL were equal to the separator temperature within a few °C. This level of temperature change does not affect the current or water distributions, and is not sufficient to change cell performance.

6. Conclusion

The basic separation and compression characteristics were measured for an electrochemical hydrogen pump that can selectively separate and compress hydrogen. The current distribution along the flow direction calculated by our simulation code of hydrogen pump agreed well to the measured current distribution by a segmented electrode cell, except when H_2 concentration is low and H_2 transport rate is high. We could thus confirm the basic operation of hydrogen pump. In the separation pump operated under atmospheric pressure down to H_2 concentration of 1% and the compression pump up to cathode pressure of 1 MPa, the open circuit voltage agreed well with the Nernst potential. More than 98% of supplied H_2 could be separated and compressed with a cell voltage of 0.06–0.15 V and current efficiency near 100%. In the H_2 compression test with the pressure ratio of 10 and the current density of 0.1 A cm^{-2}, the compressor power considering overpotential loss was equal to an adiabatic compression power with 100% adiabatic efficiency. In the future we would like to clarify further the characteristics of electrochemical hydrogen pumps for low H_2 concentration and high H_2 transport rate. Also the economical evaluation and the durability issue of hydrogen pump are required to be cleared.

Acknowledgments

This study began from a joint study with Central Japan Railway Company and proceeded with a Grant-in-Aid for Basic Research, for which the authors would like to express their gratitude.

References

[1] K. Okuya, T. Murahashi, Proceeding of 15th Annual Conference of Power & Energy Society, Institute of Electrical Engineers of Japan, #260, 2003, p. B-189.
[2] K. Mitsuda, H. Maeda, H. Urushibata, M. Enami, K. Takasu, Third FCDIC Fuel Cell Symposium, #A4-2, 1996, p. 269.
[3] N. Sekiguchi, K. Himi, M. Kadosaki, Toyama Industrial Technology Center Research Report, no. 16, II-36 (2002), vol. 17, 2003, p. IV-79.
[4] R. Tamamushi, Electrochemistry, vol. 105, Tokyo Kagaku Dojin, Tokyo, 1991, p. 193.
[5] K. Onda, K. Hattori, K. Ikeda, T. Ichihara, M. Araki, M. Terai, S. Igarashi, T. Kusada, Motoyoshi, Fuel Cell Seminar, Palm Springs, vol. 109, 2005.
[6] K. Onda, T. Masuda, S. Nagata, K. Nozaki, J. Power Sources 55 (1995) 231.
[7] K. Onda, T. Araki, T. Taniuchi, D. Sunakawa, K. Wakahara, M. Nagahama, J. Electrochem. Soc., accepted for publication.
[8] S.V. Patankar, Numerical Heat Transfer and Fluid Flow (Japanese Translation Version), Morikita Shuppan, Tokyo, 1986.
[9] D. Sunakawa, S. Oyama, T. Araki, K. Onda, Electrochemistry 74 (2006) 732.